Human Reproduction, Vol.34, No.2 pp. 235–247, 2019
Advanced Access publication on December 15, 2018 doi:10.1093/humrep/dey361

human reproduction

ORIGINAL ARTICLE ***Gynaecology***

The establishment of a mouse model of deep endometriosis

Dingmin Yan[1,†], Xishi Liu[1,2,†], and Sun-Wei Guo[1,2,*]

[1]Shanghai OB/GYN Hospital, Fudan University, Shanghai 200011, China [2]Shanghai Key Laboratory of Female Reproductive Endocrine-Related Diseases, Fudan University, Shanghai 200011, China

*Correspondence address. Shanghai Obstetrics and Gynecology Hospital, Fudan University, Shanghai 200011, China.
E-mail: hoxa10@outlook.com

Submitted on August 15, 2018; resubmitted on November 7, 2018; accepted on November 30, 2018

STUDY QUESTION: Is it possible to establish a mouse model of deep endometriosis (DE)?

SUMMARY ANSWER: A mouse DE model that is macroscopically and microscopically similar to nodular lesions in humans can be constructed in as short as 3 weeks by intraperitoneal injection of uterine fragments along with the infusion of substance P (SP) and/or calcitonin gene-related peptide (CGRP).

WHAT IS KNOWN ALREADY: Although a baboon DE model was reported 5 years ago, its prohibitive cost and demand for facilities and expertise associated with the use of non-human primates put its use out of reach for most laboratories.

STUDY DESIGN, SIZE, DURATION: A total of 48 female Balb/C mice were used for this study. Among them, 16 were randomly selected as donors that contributed uterine fragments, and the remaining 32 were recipient mice. The mice with induced endometriosis were followed up for 3–4 weeks.

PARTICIPANTS/MATERIALS, SETTING, METHODS: One day before the induction of endometriosis by intraperitoneal injection of uterine fragments, osmotic pumps were inserted into equal groups of recipient mice to infuse either sterile saline, SP, CGRP, or both SP and CGRP. The hotplate test was administrated to all mice at the baseline and before and after induction of endometriosis. Four (3 for the SP +CGRP group) weeks after induction, all mice were sacrificed. Their endometriotic lesions were excised, weighed and processed for histopathologic examination, and histochemistry, immunohistochemistry and immunofluorescence analyses of markers of proliferation, angiogenesis, epithelial–mesenchymal transition (EMT), fibroblast-to-myofibroblast transdifferentiation (FMT), smooth muscle metaplasia (SMM), mesothelial–mesenchymal transition (MMT) and endothelial–mesenchymal transition (EndoMT) were done. The extent of lesional fibrosis was evaluated by Masson trichrome staining. To further evaluate surrounding organ/tissue invasion, the peritoneal areas adhesive to the lesions were excised for immunohistochemical analysis.

MAIN RESULTS AND THE ROLE OF CHANCE: Endometriotic lesions in mice treated with SP and/or CGRP satisfied all requirements for DE, i.e. presence of endometrial epithelial and stromal cells, abundance of fibromuscular content, and encapsulation in surrounding tissues or organs. The lesion weight in the CGRP, SP and SP+CGRP groups was 1.62, 2.14 and 2.18-fold, respectively, heavier than that of control group. Concomitantly, the SP, CGRP and SP+CGRP groups had significantly shorter hotplate latency than that of control group. Lesions in mice treated with SP and/or CGRP, especially with SP+CGRP, exhibited characteristics consistent with EMT, FMT, SMM and extensive fibrosis, along with signs of MMT and EndoMT. Lesional invasion into surrounding tissues/organs was found to be 25.0, 75.0 and 87.5% in mice treated with CGRP, SP and SP+CGRP, but none in control mice.

LARGE SCALE DATA: N/A.

LIMITATIONS, REASONS FOR CAUTION: This study is limited by the use of histologic and immunohistochemistry analyses only and lacks molecular data.

WIDER IMPLICATIONS OF THE FINDINGS: The establishment of a mouse DE model supports the idea that endometriotic lesions are wounds undergoing repeated tissue injury and repair and underscores the importance of microenvironments in shaping the lesions' destiny. In addition, signs consistent with MMT and EndoMT indicate that there may be more culpable factors that still remain unidentified and

[†]These two authors contributed equally to this work.

should be pursued in the future. Moreover, the close correlation between the extent of lesional fibrosis and markers of EMT, MMT, EndoMT, FMT and SMM as shown here should facilitate our understanding of the molecular mechanisms underlying the DE pathophysiology. Since this DE model is based on a biologically plausible and evidence-backed theory, it should shed much needed insight into the molecular mechanisms underlying the pathophysiology of DE.

STUDY FUNDING/COMPETING INTEREST(S): This research was supported by Grants 81471434 (S.W.G.), 81530040 (S.W.G.), 81771553 (S.W.G.), 81671436 (X.S.L.) and 81871144 (X.S.L.) from the National Natural Science Foundation of China. None of the authors has any conflict of interest to disclose.

Key words: CGRP / deep endometriosis / endothelial–mesenchymal transition / epithelial–mesenchymal transition / fibrogenesis / fibroblast-to-myofibroblast transdifferentiation / mesothelial–mesenchymal transition / mouse model / smooth muscle metaplasia / substance P

Introduction

Among the three major subtypes of endometriosis, lesions infiltrating the peritoneum by >5 mm were originally defined as deep infiltrating endometriosis (DIE) (Koninckx and Martin, 1992) but have now been redefined as deep endometriosis (DE) (Koninckx *et al.*, 2012; Gordts *et al.*, 2017). DE is recognized as the most severe clinical form of endometriosis and its clinical management is challenging (Tosti *et al.*, 2015).

The challenge in the management of DE reflects our poor understanding of its pathophysiology, due, perhaps in no small amount, to the lack of an easily available animal model. A baboon DE model based on autologous grafting of large uterine (either endometrial or full-thickness uterine) tissues into the peritoneum and waiting for 5–6 months was reported 5 years ago (Donnez *et al.*, 2013). Although a significant step toward gaining further insight into DE pathophysiology, this model is nonetheless prohibitively costly and demands facilities and expertise for the use of non-human primates which preclude most laboratories from using it This is evidenced by the lack of any subsequent publication on its use since its publication except by the group that originally reported it. Furthermore, the lengthy induction period would preclude rapid progress and moreover, and since the uteri of the model animals have been biopsied and are thus far from intact, the model may be difficult to be justified as a model for the evaluation of dysmenorrhea or subfertility resulting from DE.

In contrast, rodent models of DE, if available, would be much more economically and logistically attractive. However, in the last 20+ years, rodent models of DE have been attempted but so far are not successful (Dr Philippe Koninckx, personal communication).

Why is the making of a DE model so challenging? To qualify for DE, the lesions need to satisfy the following four requirements (Dr Philippe Koninckx, personal communication): (R1) consist of endometrial stromal and epithelial cells; (R2) be encapsulated in surrounding tissues or organs (e.g. bowel wall, rectovaginal septum); (R3) display signs consistent with smooth muscle metaplasia (SMM); and (R4) exhibit extensive fibrosis.

All existing rodent models of endometriosis satisfy R1, and, if given longer induction period, may also satisfy R4 and perhaps R3 as well. R3 essentially requires the presence of smooth muscle-like tissues within the lesion, which can be demonstrated by the presence of cells that are morphologically similar to that of smooth muscle cells (SMCs) and also express markers of SMC, such as desmin, a marker for differentiated and mature SMC (Hasegawa *et al.*, 2003). The combination of R3 and R4 yields an endometriotic lesion that is nodular in look and feel. R2 requires the presence of adhesion in or around the lesion, and, additionally, the conjoining of endometriotic lesions and their surrounding tissues and/or organs such as mesothelium. This is referred to as 'surrounding organ invasion' (Donnez *et al.*, 2013). This can be achieved when endometriotic cells gain mobility and/or invasiveness through either epithelial–mesenchymal transition (EMT) or fibroblast-to-myofibroblast transdifferentiation (FMT)—as in wound contraction. Alternatively, when a subset of myofibroblasts are transdifferentiated from mesothelial cells through mesothelial-to-mesenchymal transition (MMT), which is an EMT-like process (Sandoval *et al.*, 2016), this encapsulation would also ensue.

Taking cues from the striking proximity of DE lesions to several nerve plexuses and from the observation that endometriotic lesions are hyperinnervated with sensory nerves (Anaf *et al.*, 2000; Berkley *et al.*, 2004; Tokushige *et al.*, 2006; Mechsner *et al.*, 2007, 2009; Wang *et al.*, 2009b; Zhang *et al.*, 2010), especially in DE lesions (Wang *et al.*, 2009a,b, Anaf *et al.*, 2011), we recently found that sensory, and to a much lesser extent sympathetic, denervation, decelerates the development of endometriosis (Liu *et al.*, unpublished data). In addition, we found that through their respective receptors, the sensory nerve-derived neuropeptides substance P (SP) and calcitonin gene-related peptide (CGRP) induce EMT, FMT and further transdifferentiation into SMCs in endometriotic lesions, resulting in extensive fibrosis (Yan *et al.*, unpublished data). These findings raise the prospect that treating mice with induced endometriosis with SP and/or CGRP may further accelerate lesion development, producing DE-like lesions.

In this study, we tested this hypothesis and present our results on the induction of DE that satisfies all four requirements for DE in mouse. We also present novel findings of MMT and evidence for endothelial–mesenchymal transition (EndoMT) in the development of DE lesions.

Materials and Methods

Animals

A total of 48 virgin female Balb/C mice, 6-week old and ~16–18 g in bodyweight, were purchased from the SLAC Experimental Animal Company (Shanghai, China) and used for this study. Among the 48 mice, 16 were randomly selected as donors that contributed uterine fragments, and the remaining 32 were recipients. All mice were maintained under controlled

conditions with a light/dark cycle of 12/12 h and had access to food and water *ad libitum*.

All experiments were performed under the guidelines of the National Research Council's *Guide for the Care and Use of Laboratory Animals* (Council, 1996) and approved by the institutional experimental animals review board of Shanghai OB/GYN Hospital, Fudan University.

Induction of endometriosis

We used an established mouse model of endometriosis by intraperitoneal (i.p.) injection of endometrial fragments (Somigliana *et al.*, 1999) as used in our previous studies (Ding *et al.*, 2015; Long *et al.*, 2016). A brief description of the procedure can be found in Supplementary Information.

DE construction

SP and CGRP (Sigma, St Louis, MO, USA) are sensory nerve-derived neuropeptides and inflammatory mediators involved in pain transmission (Henderson *et al.*, 2006; Wang *et al.*, 2009b; Ozturk *et al.*, 2010; Fisher *et al.*, 2015; Li *et al.*, 2015) and were used to accelerate lesional fibrosis and adhesion. The 32 recipient mice were randomly divided into four groups of equal sizes: control (CTL), SP, CGRP and SP+CGRP. One day before the induction of endometriosis, Alzet osmotic pumps (model 1004, DURECT Corp, Cupertino, CA, USA) were inserted in the nape of the neck (Long et al., 2016) in the groups of mice to infuse sterile saline, SP (100 μg/kg/day) (Foldenauer *et al.*, 2012), CGRP (100 μg/kg/day), or both SP (100 μg/kg/day) and CGRP (100 μg/kg/day), respectively. The pump ensured consistent and controlled release of contents with a uniform speed. Since the combined use of SP and CGRP further accelerated lesional development, mice in this group were sacrificed 1 week earlier than mice in the rest of three groups.

Baseline bodyweight and hotplate latency of all mice were evaluated and recorded before the pump insertion (Day −1), prior to endometriosis induction (Day 0), every week after the induction (Days 7, 14 and 21) and before mice were sacrificed by cervical dislocation (Day 28). The abdominal cavities were immediately opened up and all lesions were excised and processed for quantification and histological analysis. Details on hotplate test have been reported previously (Long *et al.*, 2016) and can be found in the Supplementary Information.

Quantification of lesions

After the total lesion weight was measured, the lesions were then fixed immediately in 4% (w/v) paraformaldehyde and embedded in paraffin for pathologic examination, and histological, immunohistochemistry (IHC) and immunofluorescence analyses. The endometriotic epithelium and stroma were visualized by haematoxylin and eosin (H&E) staining. The extent of fibrosis was evaluated by Masson trichrome staining. To further evaluate surrounding organ/tissue invasions, the peritoneal areas attached to the lesions were excised for immunohistochemistry analysis. The presence of surrounding organ/tissue invasion was determined as previously reported (Donnez *et al.*, 2013). Briefly, glandular infiltration was seen from the initial lesion through the peritoneal and sigmoid wall. In some cases, endometrial glands were seen to colonize the sigmoid epithelium (Supplementary Fig. S1).

Immunohistochemistry

Serial 4-μm sections were obtained from each block. The first slide was H&E stained (Sun Biotec, Shanghai, China) to confirm pathologic diagnosis and the subsequent slides for IHC analysis for proliferating cell nuclear antigen (PCNA) (1 μg/ml; Abcam, Cambridge, UK), vascular endothelial growth factor (VEGF) (2.96 μg/ml; Abcam), neurokinin 1 receptor (NK1R) (4 μg/ml; Santa Cruz), calcitonin receptor-like receptor (CRLR) (1 μg/ml, Abcam), receptor activity modifying protein 1 (RAMP1) (10 μg/ml, Abcam), E-cadherin (0.13 μg/ml, Cell Signaling Technology, Boston, MA, USA), vimentin (10 μg/ml, Abcam), α-smooth muscle actin (α-SMA) (2 μg/ml, Abcam), desmin (5 μg/ml, Abcam), smooth muscle, myosin heavy chain (SM-MHC) (1 μg/ml, Abcam), calretinin (4 μg/ml, Santa Cruz), Wilms tumor-1 (WT-1) (4 μg/m, Santa Cruz), CD31 (20 μg/ml, Abcam), fibroblast-specific protein-1 (FSP-1/ S100A4) (5 μg/ml, Abcam). NK1R is an endogenous receptor for SP, and CGRP mediates its effects through a heteromeric receptor composed of CRLR and a single transmembrane domain protein RAMP1 (Poyner *et al.*, 2002). Calretinin is a mesothelial marker (Lopez-Cabrera, 2014), and FSP-1, as a mesenchymal marker, was used to stain for fibroblasts (Sandoval *et al.*, 2016). WT-1 expressed by mesothelium regulates its functional properties during development. CD31 is used as endothelial marker, and α-SMA is stained for myofibroblasts and differentiated SMCs.

Routine deparaffinization and rehydration procedures were performed, as reported previously (Ding *et al.*, 2015). Briefly, for antigen retrieval, the slides were heated at 98°C in a citrate buffer (0.01 M, pH 6.0) for a total of 30 min for staining for PCNA, VEGF, E-cadherin, vimentin, α-SMA, desmin, SM-MHC, NK1R, CRLR, RAMP1, calretinin, FSP-1 and WT-1, or an EDTA buffer (pH 8.0, Shanghai Sun BioTech Company, Shanghai, China) for a total of 20 min for staining of CD31, and cooled naturally to room temperature. The slides were blocked with goat serum for 15 min at room temperature and then incubated with the primary antibodies overnight at 4°C. The primary antibodies were diluted in phosphate-buffered saline. After slides were rinsed with phosphate-buffered saline, they were incubated with horseradish peroxidase (HRP) labeled secondary antibody Detection Reagent (Sunpoly-HII, BioSun Technology Co., Ltd, Shanghai, China) at room temperature for 30 min. The bound antibody complexes were stained for 3–5 min or until appropriate for microscopic examination with diaminobenzidine and then counterstained with haematoxylin (30 s) and mounted. Images were obtained with the microscope (Olympus BX53, Olympus, Tokyo, Japan) fitted with a digital camera (Olympus DP73, Olympus). Three to five randomly selected images at ×400 magnification of each sample were taken to obtain a mean optional density value by Image Pro-Plus 6.0 (Media Cybernetics, Inc., Bethesda, MD, USA).

Immunofluorescence

Sections were heated for antigen retrieval in citrate buffer (0.01 M, pH 6.0), and they were incubated with 5% (v/v) goat serum for blocking non-specific binding sites. The slides were then incubated overnight at 4°C with primary antibodies, including goat anti-mouse calretinin (4 μg/ml, Santa Cruz), rabbit anti-mouse α-SMA (2 μg/ml; Abcam), mouse anti-mouse WT-1 (4 μg/ml, Santa Cruz), mouse anti-mouse CD31 (20 μg/ml, Abcam), or rabbit anti-mouse FSP-1 (10 μg/ml, Abcam) antibodies. The slides were incubated with 10 μg/ml FITC-conjugated donkey anti-goat secondary antibody (Servicebio, Wuhan, China) or 10 μg/ml Cy3-conjugated donkey anti-rabbit secondary antibody (Servicebio) or 10 μg/ml Alexa Fluor® 647-conjugated donkey anti-mouse secondary antibody (Abcam) as appropriate for 1 h at 37°C. Nuclei were counterstained with DAPI (Beyotime, Shanghai, China). Fluorescent slides were examined under a confocal laser scanning microscope (Leica TCS SP5 Confocal Microscope, Solms, Germany) at room temperature. Images were recorded separately with different objective lenses (20× and 40×/1.25-oil objective), and then exported as a TIFF-format digital file. Image-Pro Plus 6.0 was used to process the images (brightness and contrast) and to construct merged images. All images were evaluated with the same setting for brightness and contrast.

Masson trichrome staining

Masson trichrome staining was used for the detection of collagen fibers in endometriotic tissue samples. Tissue sections were deparaffinized in

xylene and rehydrated in a graded alcohol series, then were immersed in Bouin's solution (saturated picric acid 75 ml, 10% (w/v) formalin solution 25 ml and acetic acid 5 ml) at 37°C for 2 h. Sections were stained using the Masson's Trichrome Staining kit (Baso, Wuhan, China) following the manufacturer's instructions and used as previously reported (Zhang *et al.*, 2017). The areas of the collagen fiber layer stained in blue in proportion to the entire field of the ectopic endometrium were calculated by the Image Pro-Plus 6.0.

Positive and negative controls of immunohistochemistry analysis

For positive controls, mouse brain tissue samples were used for staining of NK1R, CRLR, RAMP-1 and calretinin, and human ovarian endometrioma tissue samples were used for staining of PCNA, VEGF, vimentin, α-SMA, CD31 and FSP-1 (Matsuzaki and Darcha, 2012). For staining of desmin and SM-MHC, human adenomyotic tissue samples were used, while human ovarian adenocarcinoma tissue samples were used for WT-1 (Fadare *et al.*, 2013). For negative controls, we used IgG from rabbit or mouse serum instead of the primary antibodies (Supplementary Fig. S2).

Statistical analysis

The comparison of distributions of continuous variables between or among two or more groups was made using the Wilcoxon's and Kruskal's test, respectively, and the paired Wilcoxon's test was used when the before–after (induction of endometriosis) comparison was made for the same group of subjects. Multivariate linear regression analyses were used to determine which factors were associated with lesion weight, hotplate latency or immunostaining levels.

P-values of <0.05 were considered statistically significant. All computations were made with R 3.5.1 (Team, 2016).

Results

Sensory nerve-derived neuropeptides successfully induce DE in mouse

All mice survived the experiment. There was no difference in bodyweight among the four groups at all time points (all *P*-values>0.14; Fig. 1A) and no notable adverse effect was found. Insertion of the pump appeared to reduce the bodyweight in all mice (all *P*-values

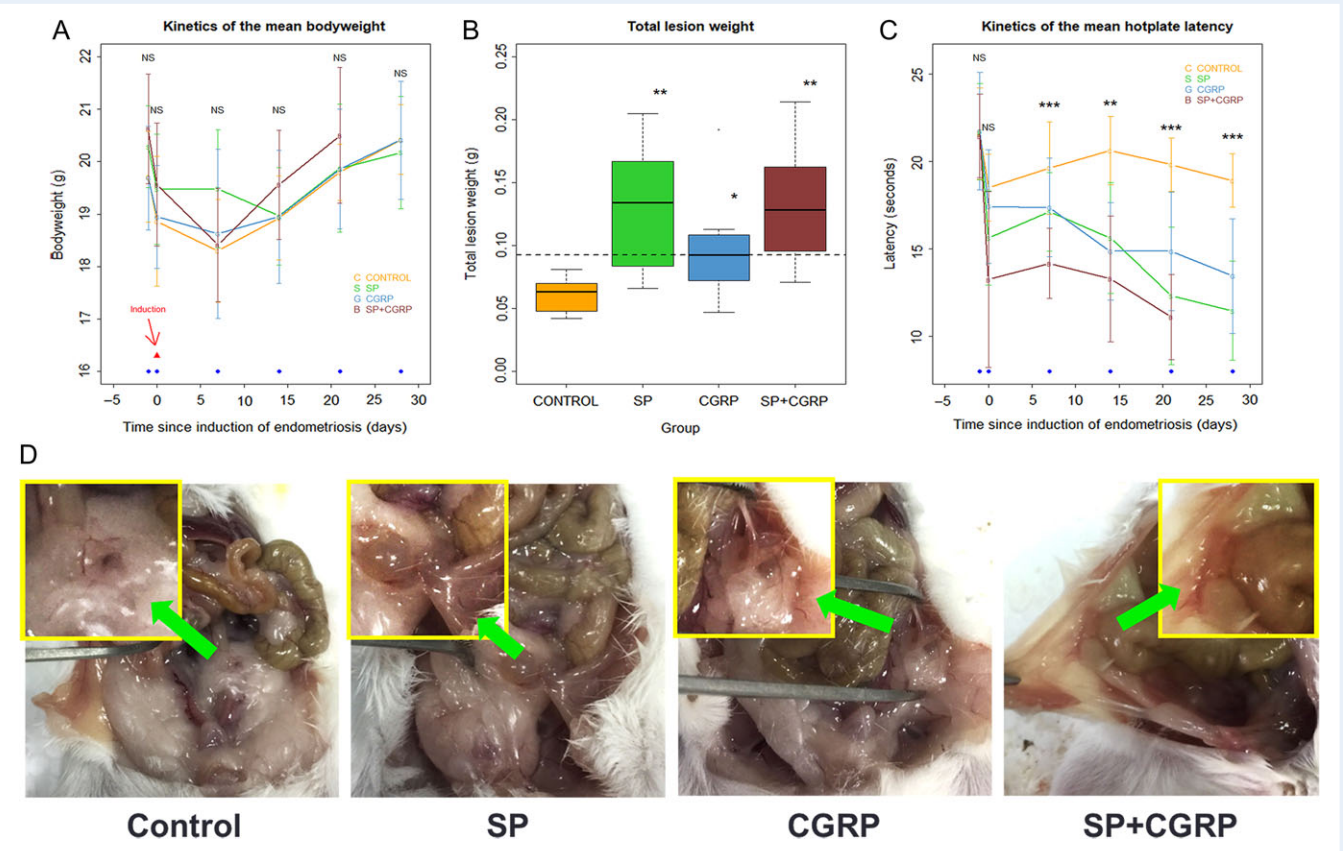

Figure 1 Summary results of the endometriosis induction experiment and the gross appearance of lesions. (**A**) The dynamic changes of the mean bodyweight in mice treated with vehicle, substance P (SP) or calcitonin gene-related peptide (CGRP) or both SP and CGRP. (**B**) Boxplot of lesion weight in different groups. The dashed line represents the median value of all groups of mice. (**C**) Kinetics of the mean hotplate latency in different groups. At all time points $n = 8$ for each group. Data are presented as mean ± SD. *$P < 0.05$; **$P < 0.01$; ***$P < 0.001$; NS: not statistically significant, i.e. $P > 0.05$, all by Kruskal's rank test (except in (B), where the comparison was made, by Wilcoxon's test, in reference to the control group). In (A), the time point at which the induction was made is indicated, and the time points at which the hotplate test was administrated are indicated by blue dots. (**D**) Gross appearance of endometriotic lesions in different groups of mice. Figures from left to right show endometriotic lesions in the abdomen of mice treated with vehicle (Control), SP, CGRP and SP+CGRP, respectively (Arrows).

Table I Summary of the location and cellular components of different immunohistochemistry markers.

Name	Cell type	Location of positive staining	Staining intensity	Scoring in which component
Neurokinin 1 receptor (NK1R)	Both in endometriotic glandular epithelial and stromal cells (mainly in epithelial cells)	Cell membrane and cytoplasm	Medium; increased after SP treatment	Glandular epithelial cells of the lesions
Calcitonin receptor-like receptor (CRLR)	Both in endometriotic glandular epithelial and stromal cells (mainly in epithelial cells)	Cell membrane and cytoplasm	Medium; increased after CGRP treatment	Glandular epithelial cells of the lesions
Receptor activity modifying protein 1 (RAMP1)	Both in endometriotic glandular epithelial and stromal cells (mainly in epithelial cells)	Cell membrane and cytoplasm	Medium; increased after CGRP treatment	Glandular epithelial cells of the lesions
Proliferating cell nuclear antigen (PCNA)	Both in endometriotic glandular epithelial and stromal cells (mainly in epithelial cells)	Cell nucleus	Strong; increased after SP and SP +CGRP treatment	Glandular epithelial cells of the lesions
Vascular endothelial growth factor (VEGF)	Glandular epithelial cells	Cytoplasm	Medium; increased after SP and CGRP treatment	Glandular epithelial cells of the lesions
E-cadherin	Glandular epithelial cells	Cytoplasm	Strong; decreased after SP and CGRP treatment	Glandular epithelial cells in lesions and adhesive lesions
Vimentin	Mesenchymal cells	Cytoplasm	Medium; increased after SP and CGRP treatment	Stromal component of lesions and adhesive lesions
α-smooth muscle actin (α-SMA)	Mesenchymal cells, also smooth muscle cells around the lesions	Cytoplasm	Strong; increased after SP and CGRP treatment	Stromal component of the lesions and mesothelium of adhesive lesions
Desmin	Smooth muscle cells	Cytoplasm	Strong; increased after SP and CGRP treatment	Stromal component of the ectopic lesions
Smooth muscle, myosin heavy chain (SM-MHC)	Smooth muscle cells	Cytoplasm	Medium; increased after SP and CGRP treatment	Stromal component of the lesions
Calretinin	Mesothelial cells	Cytoplasm	Strong; decreased after SP and CGRP treatment	Mesothelium of adhesive lesions
Wilms tumor-1 (WT-1)	Mesothelial cells	Cytoplasm	Medium; increased after SP and CGRP treatment	Mesothelium of adhesion lesions
CD31	Epithelium of blood vessels	Cell membrane	Strong; decreased after SP and CGRP treatment	Stromal component of the lesions
Fibroblast-specific protein-1 (FSP-1/ S100A4)	Mesenchymal cells	Cytoplasm and nucleus	Medium; increased after SP and CGRP treatment	Stromal component of the lesions

<0.003), until 3 weeks after the induction of endometriosis (Fig. 1A). The drop in bodyweight was most likely due to pain-suppressed appetite because the insertion was followed by a dramatic reduction in hotplate latency ($P = 3.0 \times 10^{-6}$; Fig. 1C).

Compared with controls, mice that received SP, CGRP or SP +CGRP infusion had significantly larger lesions (all $P < 0.03$; Fig. 1B). On average, the lesion weight in the SP+CGRP group was increased by 2.18-fold as compared with that of control group, while SP and CGRP infusion increased the weight by 2.14 and 1.62-fold, respectively (Fig. 1B). In addition, consistent with the human DE, the endometriotic lesions also displayed severe intraperitoneal adhesion in mice treated with SP and/or CGRP, especially in the SP and SP+CGRP groups (Fig. 1D). In both SP and SP+CGRP groups, endometriotic lesions were closely attached to the bowel wall or lateral side of peritoneum that could not be separated (Fig. 1D).

Consistent with the increased lesion weight and thus the disease severity, the SP, CGRP and SP+CGRP groups had significantly shorter hotplate latency than that of control group, starting from 2 weeks after the induction (all *P*-values <0.004), even though no difference in latency was found prior to the mini-pump insertion ($P = 0.97$; Fig. 1C). In particular, mice in the SP+CGRP group had significantly shorter latency than that of the control group starting from the day of induction (all *P*-values < 0.024; Fig. 1C). Overall, SP+CGRP mice consistently exhibited shorter latency than the other groups, and, with the only exception of the 2-week post-induction time point, SP mice had shorter latency than that of CGRP mice, although the difference did not reach statistical significance (all *P*-values >0.23).

We next evaluated the immunoreactivity against SP and CGRP respective receptors NK1R, CRLR and RAMP1 in lesions. The staining of NK1R, CRLR and RAMP1 was seen in both epithelial and stromal cells and localized in the cytomembrane (Table I). As expected, the SP and SP+CGRP, and to a less extent the CGRP, groups had significantly higher NK1R expression than that of the control group (all *P*-values <0.007; Figs 2 and 3), while the CGRP and SP+CGRP groups and, to a less extent the SP group as well, had significantly higher CRLR and RAMP1 staining levels than that of the control group (all *P*-values <0.007; Figs 2 and 3). The multiple linear regression analysis indicated that the combined treatment with SP and CGRP did not synergistically increase the staining levels of either NK1R, CRLR or RAMP1 as compared with treatment with SP or CGRP alone.

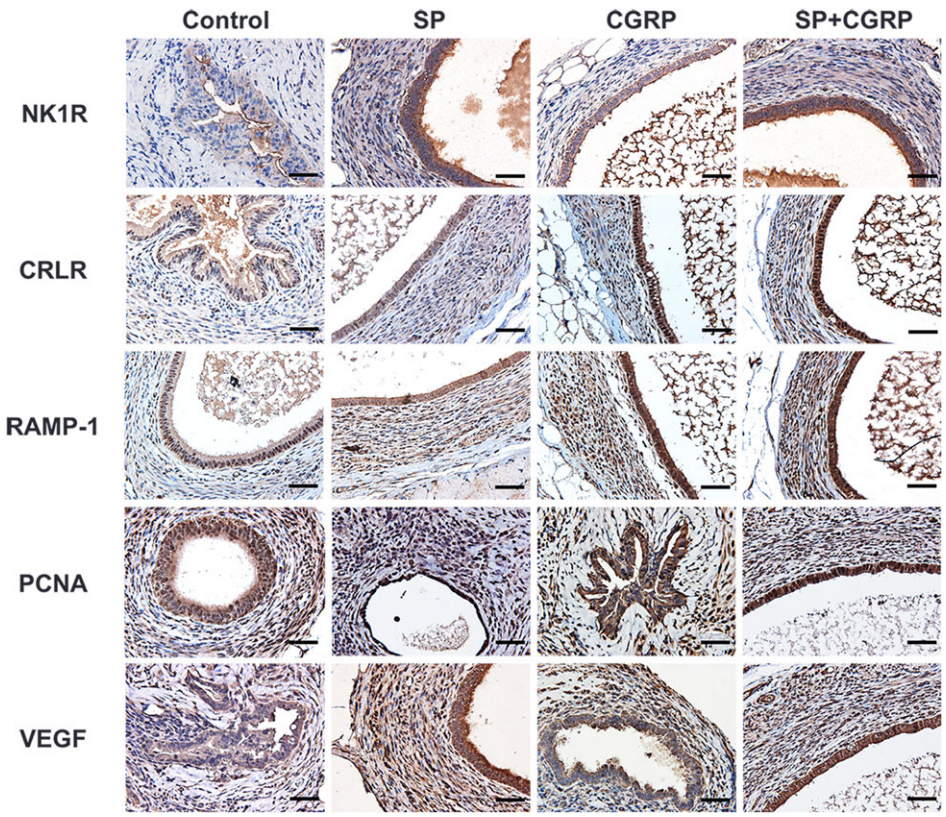

Figure 2 Representative immunostaining of NK1R, CRLR, RAMP1, PCNA, VEGF in endometriotic lesions in mice treated with vehicle, substance P (SP) or calcitonin gene-related peptide (CGRP), or SP+CGRP. Magnification: ×400. Scale bar = 50 μm.

We found that lesion PCNA immunoreactivity was localized in the cell nucleus and was seen in both glandular epithelial and stromal cells, but predominantly in glandular epithelial cells (Fig. 2). Similarly, VEGF staining was seen primarily in glandular epithelial cells and was localized in the cytoplasm. Therefore, we restricted our attention on the epithelial component of lesions. Consistent with increased lesion weight, SP and SP+CGRP groups yielded higher immunostaining levels of PCNA and VEGF as compared with controls (all *P*-values <0.002; Figs 2 and 3). With the exception of VEGF, CGRP treatment alone also yielded significantly higher PCNA staining level than that of the controls ($P = 0.037$; Figs 2 and 3), concomitant with an increased cell proliferative propensity induced by SP and/or CGRP. Multiple linear regression analyses also confirmed these findings.

Evidence for EMT, FMT, SMM and fibrosis

In mice treated with SP and/or CGRP, the E-cadherin staining levels in glandular epithelial cells were all significantly reduced as compared with that of controls (all *P*-values <0.0009; Figs 2 and 3). In contrast, the staining levels of vimentin were all significantly elevated as compared with that of the control group, especially in the SP and SP +CGRP groups (all *P*-values <0.0009; Figs 3 and 4). Taken together, these data strongly suggest the occurrence of EMT within lesions, perhaps more strongly in mice treated with SP and SP+CGRP.

We found that α-SMA-positive myofibroblasts were distributed abundantly in lesional stroma near the glandular epithelium (Table I, Figs 3 and 4). In particular, the staining of α-SMA became more widespread and intense in the stromal compartment in treated mice, especially the combined treatment even though the lesions harvested from the SP+CGRP mice were 25% 'younger' than other groups (all *P*-values <0.0002; Figs 3 and 4). This is consistent with the notion of progressive FMT in lesional development, and SP and/or CGRP facilitated this progression.

We also performed Masson trichrome staining to quantify the extent of lesional fibrosis as well as IHC analysis of desmin and SM-MHC, two markers of SMCs. In treated groups—especially the SP and SP+CGRP groups, the staining levels of both desmin and SM-MHC in the stromal compartment were significantly higher than that of controls (all *P*-values <0.0002; Figs 3 and 4), indicating a more thorough SMM in these groups. Consistent with this finding and those reported in the above, the extent of lesional fibrosis was also significantly elevated in mice treated with SP and/or CGRP, especially with SP (all *P*-values <0.001; Figs 3 and 4). Multiple linear regression analyses also confirmed these findings.

Evidence for MMT and EndoMT

We found that in the SP and SP+CGRP groups, the lesions were often closely attached to the bowel wall, or lateral side of the peritoneum

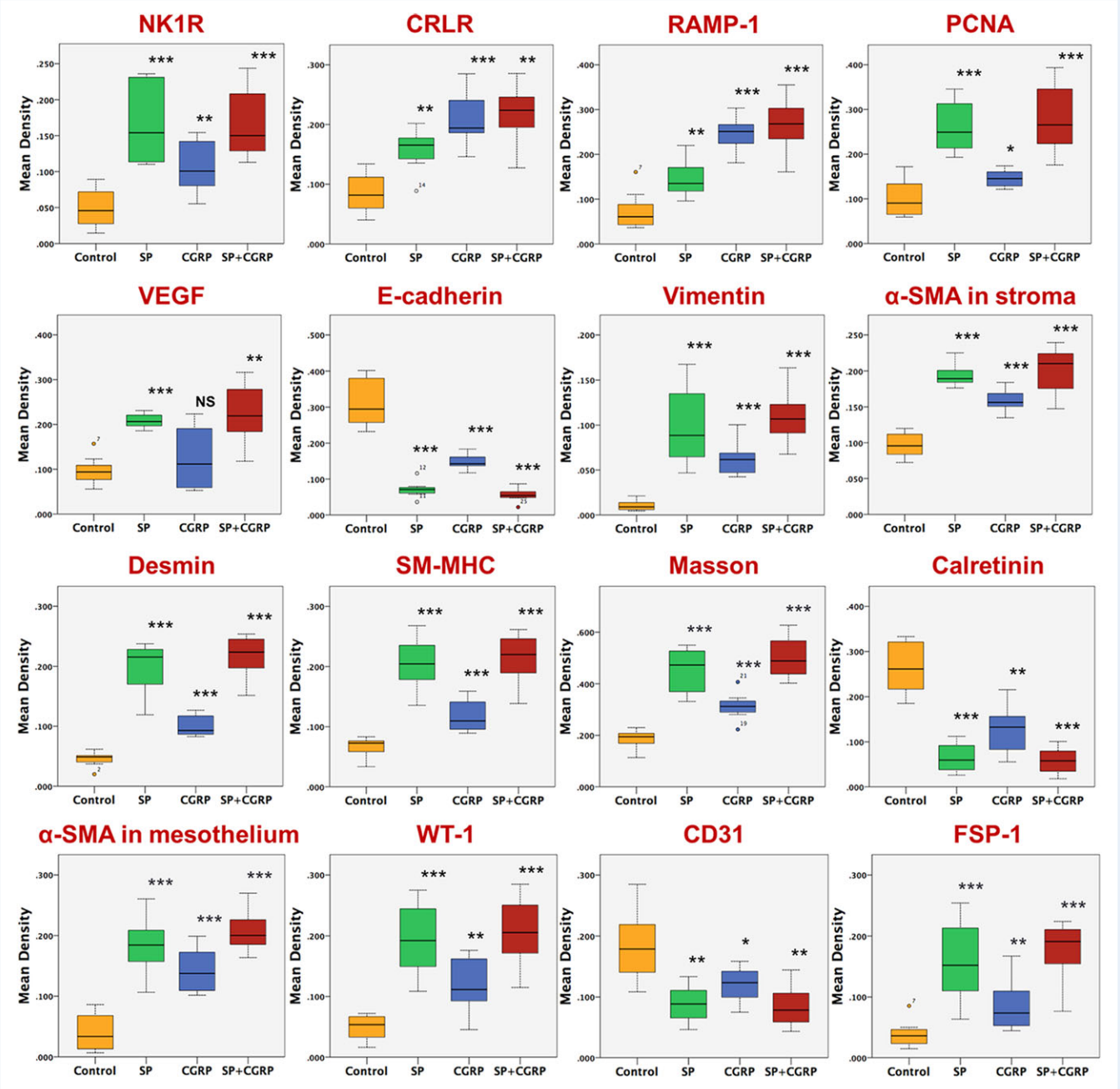

Figure 3 Summary of immunohistochemistry and histochemistry analyses by boxplots. The staining levels of NK1R, CRLR, RAMP1, PCNA, VEGF, E-cadherin and vimentin were evaluated in lesional glandular epithelium. The staining levels of α-SMA were evaluated, separately, in the lesional stromal component and surrounding mesothelium. The staining levels of desmin, SH-MHC, CD31 and FSP-1 as well as the extent of lesional fibrosis by trichrome staining were evaluated in the stromal component, and that of calretinin, α-SMA and WT-1 was evaluated in mesothelium within adhesive lesions. All comparison was made, by Wilcoxon's test, in reference to the control group. *$P < 0.05$, **$P < 0.01$, ***$P < 0.001$; NS: statistically not significant, i.e. $P > 0.05$. SP=substance P; CGRP= calcitonin gene-related peptide.

that could not be separated (Fig. 1D). The presence of glandular epithelial cells (E-cadherin-positive) and stromal (vimentin-positive) cells inside the surrounding adhesive peritoneum in six mice of SP group (75.0%; $P = 0.007$), two from the CGRP group (25.0%; $P = 0.47$) and seven from the SP+CGRP group (87.5%; $P = 0.0014$), but none in the control group (0.0%) (Fig. 5). This observation indicates that requirement R2 was met.

Since adhesion is ubiquitous in endometriotic lesions, we wondered whether MMT occurred in the putative DE lesions. Accordingly, we evaluated the expression of calretinin, α-SMA and WT-1 in mesothelial cells by immunohistochemistry analysis. We found abundant α-SMA-positive myofibroblasts with submesothelial localization and even some α-SMA-positive mesothelial cells in lesions from SP, CGRP and SP+CGRP mice (Fig. 5). In contrast to its presence in many stromal

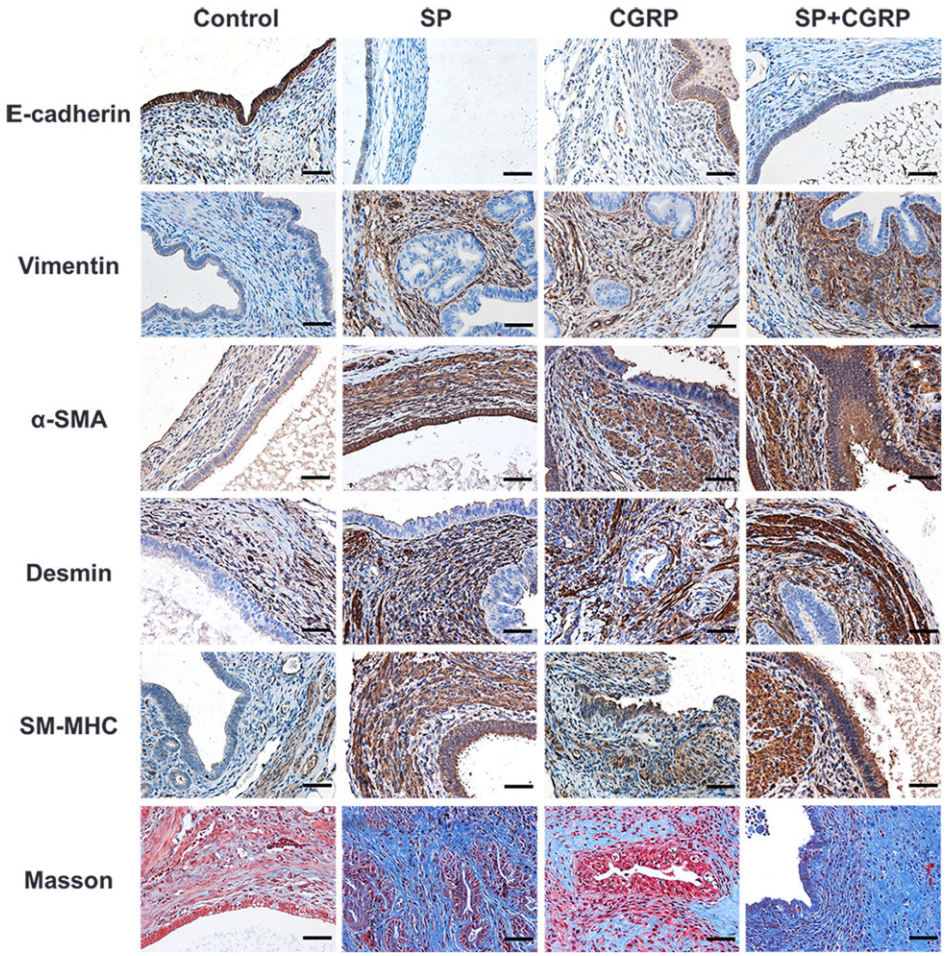

Figure 4 Representative photomicrographs of immunohistochemistry and histochemistry (Masson trichrome) analyses of E-cadherin, vimentin, α-SMA, desmin and SM-MHC, along with the extent of fibrosis in endometriotic lesions of different groups. Magnification: ×400. Scale bar = 50 μm. SP=substance P; CGRP= calcitonin gene-related peptide.

cells/fibroblast-like cells, the staining of calretinin, a marker for peritoneal mesothelial cells, localized in the cytoplasm in the mesothelium within lesions was significantly reduced in SP- and/or CGRP-treated mice versus the control group (*P*-values ≤0.002; Figs 2 and 5). As expected, the stromal WT-1 staining levels were higher in the mesothelium in adhesive lesions from mice treated with SP, CGRP and SP +CGRP groups as compared with the controls, especially in the SP and SP+CGRP groups (*P*-values ≤0.003; Figs 2 and 5).

We also found evidence for EndoMT-like changes in endometriotic lesions. Since the defining feature of EndoMT is the expression of mesenchymal markers in endothelial cells, we stained both FSP-1, which is typically expressed in mesenchymal cells, and CD31, a marker for endothelial cells, in the stromal component (Table I). FSP-1 staining was localized in the cytoplasm and nucleus of mesenchymal cells in lesions, but was increasingly intense in the epithelial/mesothelial component as the lesions became more fibrotic, suggestive of MMT/EMT. CD31 immunostaining was seen mostly in vascular endothelial cells in lesional stroma. Concomitant with the decreased CD31-positive endothelial cells (all *P*-values <0.021), there was an elevated staining of FSP-1 under SP and/or CGRP treatment (all *P*-values <0.0014; Figs 3 and 4). These results demonstrate that SP may have precipitated MMT and EndoMT in the development of DE-like lesions in mouse.

To further confirm the occurrence of MMT and EndoMT in putative DE lesions, we double-stained calretinin and α-SMA or FSP-1 via immunofluorescence in endometriotic lesions. Through laser scanning confocal microscopy, we found that, while lesions in the control group and, to a much less extent, the CGRP group, still retained the expression of calretinin, those from the SP and SP+CGRP groups had lost it and had acquired the mesenchymal/myofibroblast phenotype as seen by the positive staining of FSP-1 and α-SMA in the mesothelial monolayer (Fig. 6A and B).

We also further confirmed EndoMT-like changes by immunofluorescence. We found co-localization of endothelial (CD31) and mesenchymal (FSP-1) markers in the SP-treated endometriotic lesions, with a decrease of CD31 expression and an increase of FSP-1 staining, but not in lesions from CGRP or control group (Fig. 6C). Thus, we provide the first piece of evidence that MMT and EndoMT occurred in our mouse DE model, and SP and/or CGRP promoted the fibrogenic processes in endometriotic lesions, resulting in DE.

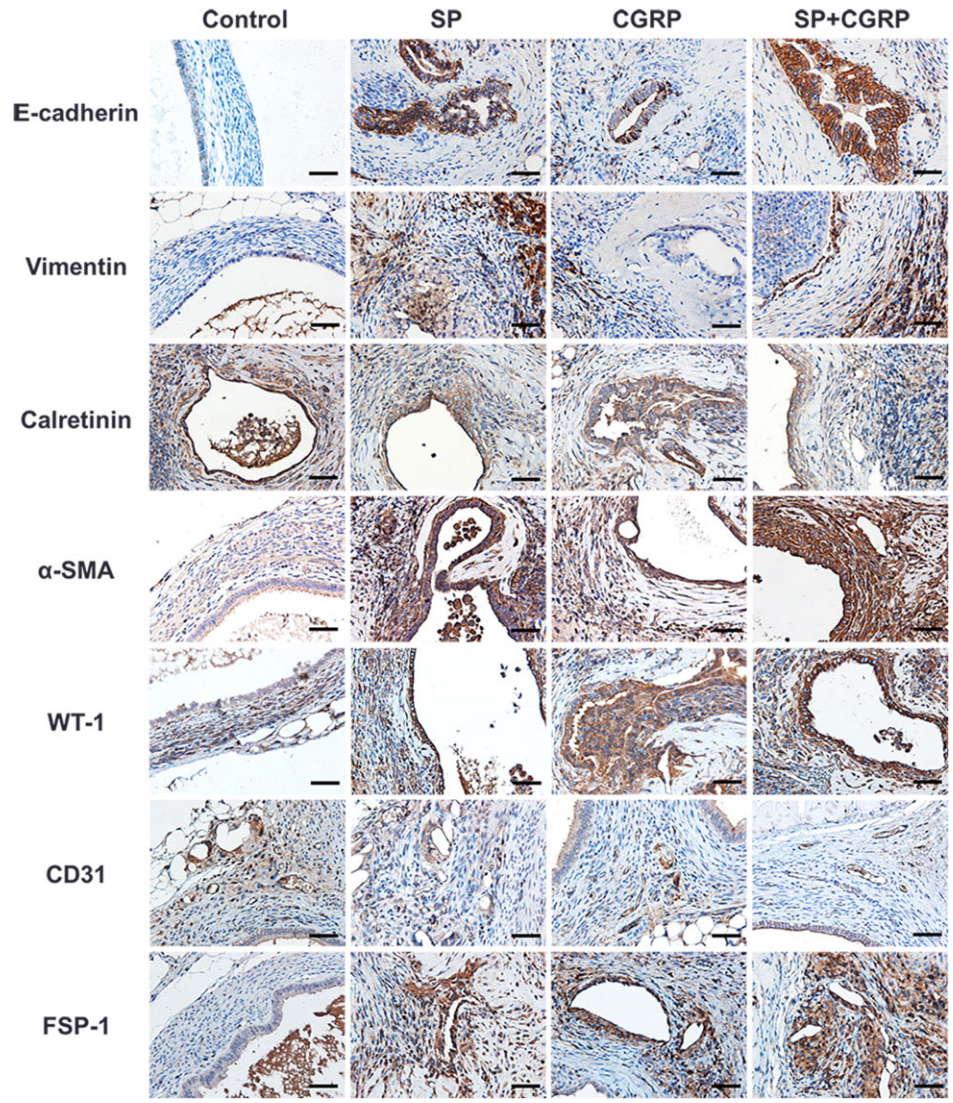

Figure 5 Representative immunostaining of E-cadherin, vimentin, calretinin, α-SMA, WT-1, CD31 and FSP-1 in adhesive lesions from different groups of mice. Magnification: ×400. Scale bar = 50 μm. SP=substance P; CGRP= calcitonin gene-related peptide.

Correlates of hotplate latency and lesional fibrosis

Since pain is typically the main reason that brings patients to medical attention, we evaluated what parameters were correlated with the hotplate latency. We found that the latency was negatively correlated with the lesion weight ($r = -0.50$, $P = 0.004$; Fig. 7). The latency also correlated with the extent of lesional fibrosis ($r = -0.68$, $P = 1.8 \times 10^{-5}$; Fig. 7), suggesting that the latter may be more important than the lesion size in determining the degree of hyperalgesia in mouse with induced endometriosis.

Given that these markers for EMT, FMT and SMM that are known to be involved in lesional development, which ends with fibrosis, we further evaluated their relationship, if any, with the extent of fibrosis. We found that the extent of fibrosis correlated closely with markers of EMT, FMT and SMM, and also correlated with the lesional expression levels of NK1R, CRLR and RAMP1 (Fig. 7).

The staining levels of the two CGRP receptors correlated very closely ($r = 0.88$, $P = 2.1 \times 10^{-11}$; Fig. 7). They also correlated with NK1R (r's > 0.70, P's < 2.0×10^{-6}).

Discussion

In this study, by using intraperitoneal injection of uterine fragments in conjunction with the infusion of SP and/or CGRP, we have developed a mouse DE model that is macroscopically and microscopically similar to the nodular lesions in humans. The model met all four requirements for DE. The induction procedure requires no surgery, the model is easy to establish, inexpensive, and can be established in as short as 3 weeks. Any laboratory with a mouse facility should be able to use this model. Additionally, the use of hotplate latency as a surrogate for DE-associated pain enhances its utility as a mouse model for preclinical research. Moreover, the close correlation between the extent of

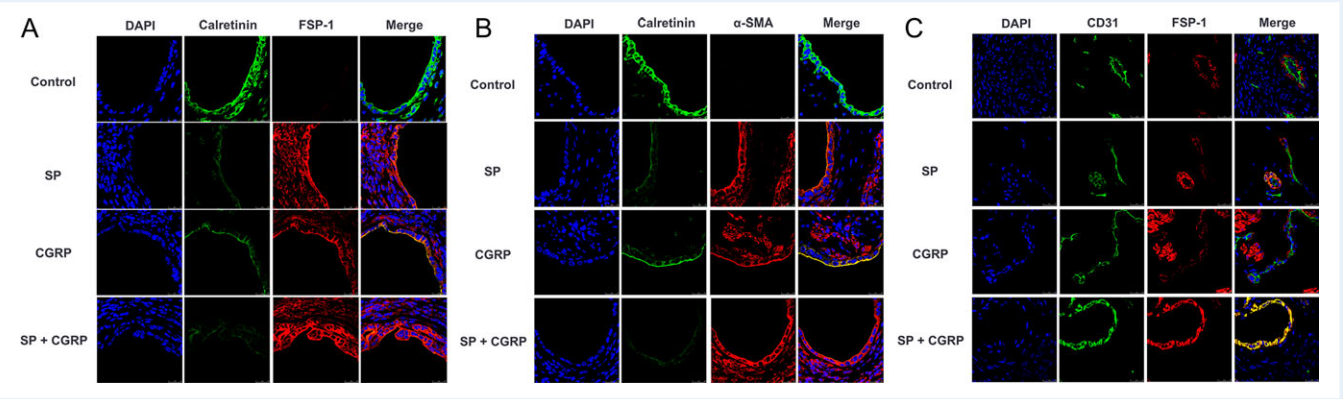

Figure 6 Representative photomicrographs of immunofluorescence staining suggestive of the occurrence of MMT and EndoMT in endometriotic lesions. In mice treated with substance P (SP) and SP + calcitonin gene-related peptide (CGRP) the mesothelium apparently lost its mesothelial marker (calretinin) and acquired the mesenchymal/myofibroblast phenotype as seen by the positive staining of FSP-1 (**A**) and α-SMA (**B**) in the mesothelial monolayer. Mice treated with CGRP still retained the calretinin expression and were also positively stained with FSP-1 (A) and α-SMA (B), suggesting partial MMT. (**C**) Lesions from mice treated with SP and SP+CGRP show co-localization of endothelial (CD31) and mesenchymal (FSP-1) markers in the stromal component. Magnification: ×400. Scale bar = 25 μm.

lesional fibrosis and markers of EMT, MMT, EndoMT, FMT and SMM as shown here should facilitate our understanding of the molecular mechanisms underlying the DE pathophysiology.

Despite all the phenotypic and clinical differences, all subtypes of endometriosis do share one single defining common denominator: as ectopic endometrium, they all undergo cyclic bleeding as eutopic endometrium (Brosens, 1997). As such, they are fundamentally wounds undergoing repeated tissue injury and repair (ReTIAR) (Guo *et al.*, 2015; Zhang et al., 2016a). Consequently, endometriotic lesions undergo EMT and FMT, resulting in increased cellular contractility and collagen production, leading ultimately to fibrosis (Zhang *et al.*, 2016b; Duan *et al.*, 2018). Prolonged exposure to activated platelets also leads to increased expression of α-SMA as well as markers of differentiated SMCs in endometriotic stromal cells, accounting for SMM. Taken together, these data confirmed that EMT, FMT, SMM and fibrogenesis are involved in lesional development (Zhang *et al.*, 2016b). In particular, SP and, to a lesser extent, CGRP accelerate the lesional development through more thorough EMT, FMT, SMM and fibrogenesis. Considering the fact that the tissue samples from mice in the SP +CGRP group were harvested one week earlier yet exhibit more extensive fibrosis, SP and CGRP synergistically promote this acceleration in lesional progression.

Our previous attempt to characterize OE and DE lesions by IHC and histological means (Liu *et al.*, 2018) gives credence to ReTIAR, and the successful construction of the mouse DE model lends further support for this notion, and also further underscores the importance of the lesional microenvironment in shaping the lesional fate. Moreover, our study presents evidence, for the first time, for the roles of MMT and EndoMT in the development of endometriosis, which so far have received scant attention.

It has long been postulated that OE, DE and superficial peritoneal endometriosis are three separate disease entities, and, as such, possibly have different pathogenesis and pathophysiology (Nisolle and Donnez, 1997). However, many similarities shared by both OE and DE as shown previously indicate that the two, and likely three, conditions may actually share the same pathogenesis/pathophysiology (Liu *et al.*, 2018). This study further provides evidence in support for the common pathophysiology shared by OE and DE, and likely other subtypes of endometriosis. Differences between them may stem from the different lesional microenvironments.That is, the determining factor in shaping the fate and destiny of endometriotic lesions is simply the location, or the lesional microenvironment.

Whether by surgical induction or intraperitoneal injection, the induction of endometriosis in rodents frequently uses the full-thickness of uterine tissue fragments (except (Greaves *et al.*, 2014) and (King *et al.*, 2016), which use endometrial fragments shed from artificially induced menstruation), due mostly to the difficulty in separating endometrial tissues from the rest of the uterine tissues. So why the grafting of the same type of tissues can result in DE lesions in baboons but not in rodents? Differences in species aside, the duration of induction period may also be responsible: the induction duration in rodents is typically 2–4 weeks, possibly not long enough to allow fibrosis to be fully developed (Zhang *et al.*, 2017). This may be consistent with the well-documented diagnostic delay in DE (Sinaii *et al.*, 2002). Moreover, the progression towards a DE lesion could well require additional push, and in this case sensory nerve-derived neuropeptides such as SP act to further expedite lesional development towards nodular lesions encapsulated in the surrounding organs or tissues.

DE lesions frequently involve implants invading the wall of the pelvic organ and thus display extensive adhesion (Vercellini *et al.*, 2004). Defined as abnormal fibrous connections joining tissue surfaces at non-anatomic locations, adhesion is formed between adjacent tissues and organs that are injured and is a sequel of the healing process (Awonuga *et al.*, 2009). Adhesion distorts anatomical structure and may contribute to pain and presents significant challenges to surgeons. It is well documented that peritoneal adhesion involves mesothelial cells that line the peritoneal cavity and form a monolayer with visceral and parietal surfaces covering the internal organs and body wall, respectively (Braun and Diamond, 2014). They play critical roles in the maintenance of serosal homeostasis in response to injury,

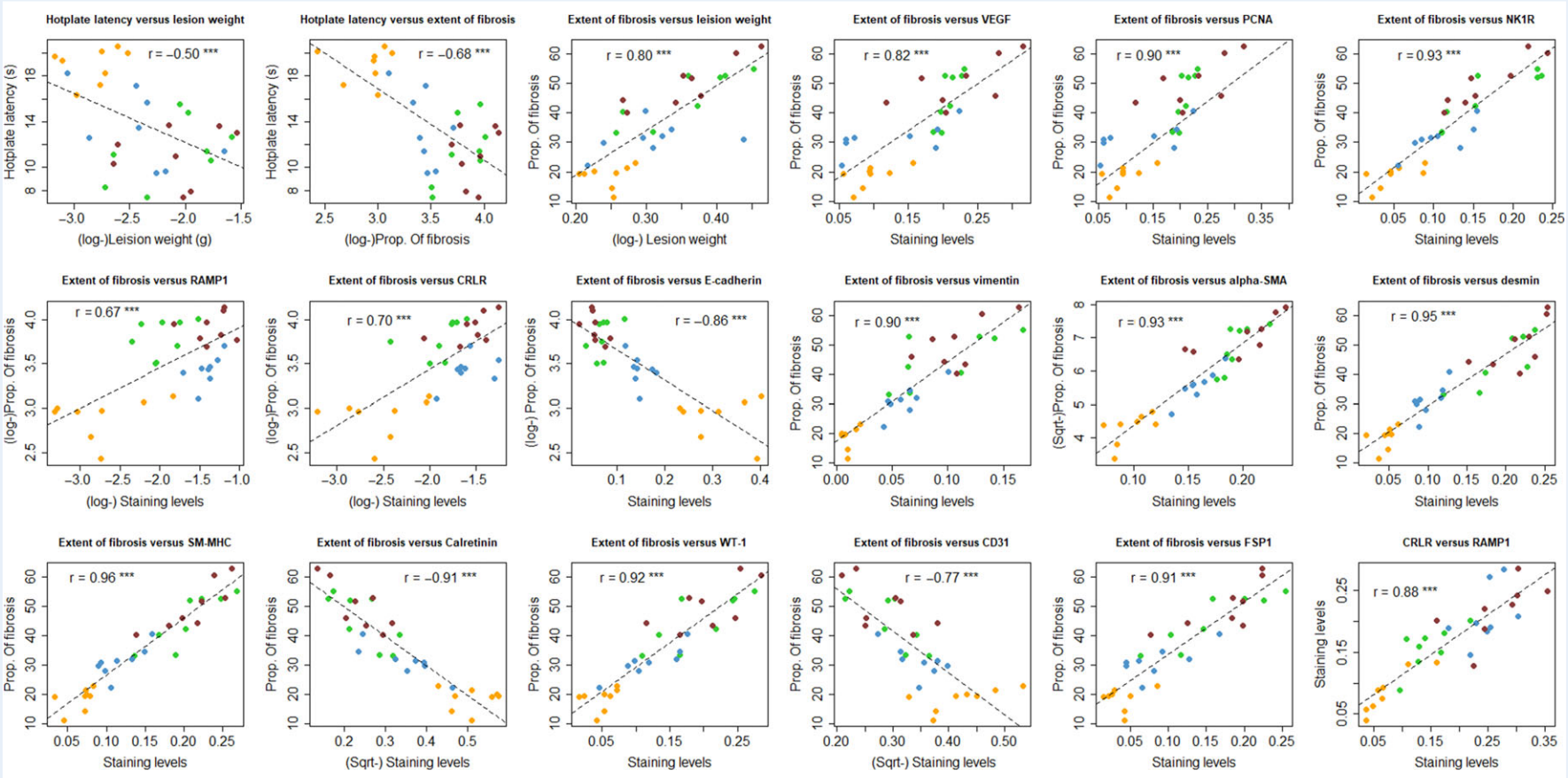

Figure 7 Scatter plots showing the relationship between hotplate latency and lesion weight, between hotplate latency and the extent of lesional fibrosis, and between the extent of lesional fibrosis and staining levels of various markers for proliferation, angiogenesis, EMT, MMT, FMT and SMM as indicated in the figures. The last plot shows the relationship between the immunostaining levels of CRLR and of RAMP1. Each dot represents 1 data point from a mouse, with different colors representing different groups: The brown color of indicates mouse from the substance P (SP) + calcitonin gene-related peptide (CGRP) group, the lime green color, the SP group, the steel blue color, the CGRP group, and the orange color, the control group. The dashed line is the regression line. The number in each figure is Pearson correlation coefficient, followed by the symbol indicating the statistical significance level. ***$P < 0.001$.

inflammation and immunoregulation. Recent research indicates that mesothelial cells can differentiate into mesenchymal cells through MMT (Sandoval *et al.*, 2016). This seems to suggest that the mesothelium is a likely source of fibrogenic cells during serosal inflammation and tissue repair and, as such, may play important roles in peritoneal fibrosis and adhesion formation (Mutsaers *et al.*, 2015). Indeed, it has been hypothesized that mesothelial cells may be a source of (myo) fibroblasts in interstitial lung fibrosis (Zolak *et al.*, 2013). Our study provides the first piece of evidence that MMT may also be involved in lesional fibrogenesis and adhesion in endometriosis. Further investigation is underway to elucidate its underlying molecular mechanisms.

Similar to mesothelial cells, endothelial cells may contribute to fibrosis through the process of EndoMT, which is originally described in experimental wound repair (Romero *et al.*, 1997). In murine models of cardiac (Zeisberg *et al.*, 2007) and lung fibrosis (Hashimoto *et al.*, 2010), endothelial cells are reported to contribute to the pool of fibroblasts. As in EMT, TGF-β1, TNF-α and IL-1β are the main drivers of EndoMT, suggesting mechanistic similarities between the two processes (Rieder *et al.*, 2011). While our data are not conclusive, at least they suggest the possibility of the involvement of EndoMT in the development of endometriosis. Further research into this area is warranted.

Granted, our DE model may still not be optimal, and further modifications could make it more efficient. In addition, whether the model has any translational value remains unclear. 'All models are wrong, but some are useful' (Box, 1979). Due to the vast differences in physiology, the mouse or perhaps even baboon models of DE may still not recapitulate all features of its human counterpart. However, as long as the model could help us understand one or more aspects of the disease, it may still be useful.

In conclusion, we have developed the first mouse model for DE. The model is easy to implement and inexpensive, and takes as little as 3 weeks to establish. In conjunction with easily measurable pain proxy measures and a battery of lesional biomarkers representing various processes that drive lesional development, this model should help shed more light on the pathophysiology of DE and facilitate its preclinical research. Above all, the successful establishment of this DE model lends further support for the notion that endometriotic lesions are wounds undergoing ReTIAR. Arguably, if we can generate a theory-guided DE model at will, then we are much closer to the day when we can develop more effective therapeutics and intervention measures for the disease.

Supplementary data

Supplementary data are available at *Human Reproduction* online.

Acknowledgements

The authors would like to Professor Philippe Koninckx for sharing his expert views on deep endometriosis and stimulating and fruitful discussions.

Authors' roles

S.W.G. conceived and designed the study, performed data analysis and data interpretation, and drafted the article. X.S.L. and D.Y. performed all the experiments and carried out data analysis. All participated in the writing and approved the final version of the article.

Funding

National Science Foundation of China (81471434, 81530040 and 81771553 to S.W.G.; 81671436 and 81871144 to X.S.L.) and an Excellence in Centers of Clinical Medicine grant (2017ZZ01016) from the Science and Technology Commission of Shanghai Municipality.

Conflict of interest

All authors state that they have nothing to declare.

References

Anaf V, El Nakadi I, De Moor V, Chapron C, Pistofidis G, Noel JC. Increased nerve density in deep infiltrating endometriotic nodules. *Gynecol Obstet Invest* 2011;**71**:112–117.

Anaf V, Simon P, El Nakadi I, Fayt I, Buxant F, Simonart T, Peny MO, Noel JC. Relationship between endometriotic foci and nerves in rectovaginal endometriotic nodules. *Hum Reprod* 2000;**15**:1744–1750.

Awonuga AO, Saed GM, Diamond MP. Laparoscopy in gynecologic surgery: adhesion development, prevention, and use of adjunctive therapies. *Clin Obstet Gynecol* 2009;**52**:412–422.

Berkley KJ, Dmitrieva N, Curtis KS, Papka RE. Innervation of ectopic endometrium in a rat model of endometriosis. *Proc Natl Acad Sci USA* 2004; **101**:11094–11098.

Box GEP. Robustness in the strategy of scientific model building. In: Launer RL, Wilkinson GN (eds). *Robustness in Statistics*. New York: Academic Press, 1979, 201–236.

Braun KM, Diamond MP. The biology of adhesion formation in the peritoneal cavity. *Semin Pediatr Surg* 2014;**23**:336–343.

Brosens IA. Endometriosis—a disease because it is characterized by bleeding. *Am J Obstet Gynecol* 1997;**176**:263–267.

Council NR. *Guide for the Care and Use of Laboratory Animals*. Washington, DC: National Academies Press, 1996.

Ding D, Liu X, Duan J, Guo SW. Platelets are an unindicted culprit in the development of endometriosis: clinical and experimental evidence. *Hum Reprod* 2015;**30**:812–832.

Donnez O, Van Langendonckt A, Defrere S, Colette S, Van Kerk O, Dehoux JP, Squifflet J, Donnez J. Induction of endometriotic nodules in an experimental baboon model mimicking human deep nodular lesions. *Fertil Steril* 2013;**99**:783–789 e783.

Duan J, Liu X, Guo S-W. The M2a macrophage subset may be critically involved in fibrogenesis of endometriosis in mouse. *Reprod Biomed Online* 2018. ;**37**:254–268.

Fadare O, James S, Desouki MM, Khabele D. Coordinate patterns of estrogen receptor, progesterone receptor, and Wilms tumor 1 expression in the histopathologic distinction of ovarian from endometrial serous adenocarcinomas. *Ann Diagn Pathol* 2013;**17**:430–433.

Fisher PW, Zhao Y, Rico MC, Massicotte VS, Wade CK, Litvin J, Bove GM, Popoff SN, Barbe MF. Increased CCN2, substance P and tissue fibrosis are associated with sensorimotor declines in a rat model of repetitive overuse injury. *J Cell Commun Signal* 2015;**9**:37–54.

Foldenauer ME, McClellan SA, Barrett RP, Zhang Y, Hazlett LD. Substance P affects growth factors in Pseudomonas aeruginosa-infected mouse cornea. *Cornea* 2012;**31**:1176–1188.

Gordts S, Koninckx P, Brosens I. Pathogenesis of deep endometriosis. *Fertil Steril* 2017;**108**:872–885 e871.

Greaves E, Cousins FL, Murray A, Esnal-Zufiaurre A, Fassbender A, Horne AW, Saunders PT. A novel mouse model of endometriosis mimics human phenotype and reveals insights into the inflammatory contribution of shed endometrium. *Am J Pathol* 2014;**184**:1930–1939.

Guo SW, Ding D, Shen M, Liu X. Dating endometriotic ovarian cysts based on the content of cyst fluid and its potential clinical implications. *Reprod Sci* 2015;**22**:873–883.

Hasegawa T, Hasegawa F, Hirose T, Sano T, Matsuno Y. Expression of smooth muscle markers in so called malignant fibrous histiocytomas. *J Clin Pathol* 2003;**56**:666–671.

Hashimoto N, Phan SH, Imaizumi K, Matsuo M, Nakashima H, Kawabe T, Shimokata K, Hasegawa Y. Endothelial-mesenchymal transition in bleomycin-induced pulmonary fibrosis. *Am J Respir Cell Mol Biol* 2010;**43**:161–172.

Henderson J, Terenghi G, McGrouther DA, Ferguson MW. The reinnervation pattern of wounds and scars may explain their sensory symptoms. *J Plast Reconstr Aesthet Surg* 2006;**59**:942–950.

King CM, Barbara C, Prentice A, Brenton JD, Charnock-Jones DS. Models of endometriosis and their utility in studying progression to ovarian clear cell carcinoma. *J Pathol* 2016;**238**:185–196.

Koninckx PR, Martin DC. Deep endometriosis: a consequence of infiltration or retraction or possibly adenomyosis externa? *Fertil Steril* 1992;**58**:924–928.

Koninckx PR, Ussia A, Adamyan L, Wattiez A, Donnez J. Deep endometriosis: definition, diagnosis, and treatment. *Fertil Steril* 2012;**98**:564–571.

Li R, Qi F, Zhang J, Ji Y, Zhang D, Shen Z, Lei W. Antinociceptive effects of dexmedetomidine via spinal substance P and CGRP. *Transl Neurosci* 2015;**6**:259–264.

Liu X, Zhang Q, Guo SW. Histological and immunohistochemical characterization of the similarity and difference between ovarian endometriomas and deep infiltrating endometriosis. *Reprod Sci* 2018;**25**:329–340.

Long Q, Liu X, Guo SW. Surgery accelerates the development of endometriosis in mouse. *Am J Obstet Gynecol* 2016;**215**:320, e1–320.e15.

Matsuzaki S, Darcha C. Epithelial to mesenchymal transition-like and mesenchymal to epithelial transition-like processes might be involved in the pathogenesis of pelvic endometriosis. *Hum Reprod* 2012;**27**:712–721.

Mechsner S, Kaiser A, Kopf A, Gericke C, Ebert A, Bartley J. A pilot study to evaluate the clinical relevance of endometriosis-associated nerve fibers in peritoneal endometriotic lesions. *Fertil Steril* 2009;**92**:1856–1861.

Mechsner S, Schwarz J, Thode J, Loddenkemper C, Salomon DS, Ebert AD. Growth-associated protein 43-positive sensory nerve fibers accompanied by immature vessels are located in or near peritoneal endometriotic lesions. *Fertil Steril* 2007;**88**:581–587.

Mutsaers SE, Birnie K, Lansley S, Herrick SE, Lim CB, Prele CM. Mesothelial cells in tissue repair and fibrosis. *Front Pharmacol* 2015;**6**:113.

Nisolle M, Donnez J. Peritoneal endometriosis, ovarian endometriosis, and adenomyotic nodules of the rectovaginal septum are three different entities. *Fertil Steril* 1997;**68**:585–596.

Ozturk N, Erin N, Tuzuner S. Changes in tissue substance P levels in patients with carpal tunnel syndrome. *Neurosurgery* 2010;**67**:1655–1660. discussion 1660-1651.

Rieder F, Kessler SP, West GA, Bhilocha S, de la Motte C, Sadler TM, Gopalan B, Stylianou E, Fiocchi C. Inflammation-induced endothelial-to-mesenchymal transition: a novel mechanism of intestinal fibrosis. *Am J Pathol* 2011;**179**:2660–2673.

Romero LI, Zhang DN, Herron GS, Karasek MA. Interleukin-1 induces major phenotypic changes in human skin microvascular endothelial cells. *J Cell Physiol* 1997;**173**:84–92.

Sandoval P, Jimenez-Heffernan JA, Guerra-Azcona G, Perez-Lozano ML, Rynne-Vidal A, Albar-Vizcaino P, Gil-Vera F, Martin P, Coronado MJ, Barcena C *et al*. Mesothelial-to-mesenchymal transition in the pathogenesis of post-surgical peritoneal adhesions. *J Pathol* 2016;**239**:48–59.

Sinaii N, Cleary SD, Ballweg ML, Nieman LK, Stratton P. High rates of autoimmune and endocrine disorders, fibromyalgia, chronic fatigue syndrome and atopic diseases among women with endometriosis: a survey analysis. *Hum Reprod* 2002;**17**:2715–2724.

Somigliana E, Vigano P, Rossi G, Carinelli S, Vignali M, Panina-Bordignon P. Endometrial ability to implant in ectopic sites can be prevented by interleukin-12 in a murine model of endometriosis. *Hum Reprod* 1999;**14**:2944–2950.

Team RDC. *R: A Language and Environment for Statistical Computing*. 2016. R Foundation for Statistical Computing, Vienna, Austria.

Tokushige N, Markham R, Russell P, Fraser IS. Nerve fibres in peritoneal endometriosis. *Hum Reprod* 2006;**21**:3001–3007.

Tosti C, Pinzauti S, Santulli P, Chapron C, Petraglia F. Pathogenetic mechanisms of deep infiltrating endometriosis. *Reprod Sci* 2015;**22**:1053–1059.

Vercellini P, Frontino G, Pietropaolo G, Gattei U, Daguati R, Crosignani PG. Deep endometriosis: definition, pathogenesis, and clinical management. *J Am Assoc Gynecol Laparosc* 2004;**11**:153–161.

Wang G, Tokushige N, Markham R, Fraser IS. Rich innervation of deep infiltrating endometriosis. *Hum Reprod* 2009a;**24**:827–834.

Wang G, Tokushige N, Russell P, Dubinovsky S, Markham R, Fraser IS. Hyperinnervation in intestinal deep infiltrating endometriosis. *J Minim Invasive Gynecol* 2009b;**16**:713–719.

Zeisberg EM, Tarnavski O, Zeisberg M, Dorfman AL, McMullen JR, Gustafsson E, Chandraker A, Yuan X, Pu WT, Roberts AB *et al*. Endothelial-to-mesenchymal transition contributes to cardiac fibrosis. *Nat Med* 2007;**13**:952–961.

Zhang Q, Duan J, Liu X, Guo SW. Platelets drive smooth muscle metaplasia and fibrogenesis in endometriosis through epithelial-mesenchymal transition and fibroblast-to-myofibroblast transdifferentiation. *Mol Cell Endocrinol* 2016a;**428**:1–16.

Zhang Q, Duan J, Olson M, Fazleabas A, Guo SW. Cellular changes consistent with epithelial-mesenchymal transition and fibroblast-to-myofibroblast transdifferentiation in the progression of experimental endometriosis in baboons. *Reprod Sci* 2016b;**23**:1409–1421.

Zhang Q, Liu X, Guo SW. Progressive development of endometriosis and its hindrance by anti-platelet treatment in mice with induced endometriosis. *Reprod Biomed Online* 2017;**34**:124–136.

Zhang X, Yao H, Huang X, Lu B, Xu H, Zhou C. Nerve fibres in ovarian endometriotic lesions in women with ovarian endometriosis. *Hum Reprod* 2010;**25**:392–397.

Zolak JS, Jagirdar R, Surolia R, Karki S, Oliva O, Hock T, Guroji P, Ding Q, Liu RM, Bolisetty S *et al*. Pleural mesothelial cell differentiation and invasion in fibrogenic lung injury. *Am J Pathol* 2013;**182**:1239–1247.